Monthly Notices
of the
ROYAL ASTRONOMICAL SOCIETY

MNRAS **491,** 1771–1776 (2020)
Advance Access publication 2019 November 6

doi:10.1093/mnras/stz3106

Polarimetry of relativistic tidal disruption event Swift J2058+0516

K. Wiersema,[1,2]★ A. B. Higgins,[2] A. J. Levan,[1,3] R. A. J. Eyles,[2] R. L. C. Starling,[2] N. R. Tanvir,[2] S. B. Cenko,[4,5] A. J. van der Horst,[6,7] B. P. Gompertz,[1] J. Greiner[8] and D. R. Pasham[9]

[1]*Department of Physics, University of Warwick, Coventry CV4 7AL, UK*
[2]*University of Leicester, University Road, Leicester LE1 7RH, UK*
[3]*Department of Astrophysics/IMAPP, Radboud University, NL-6500GL Nijmegen, the Netherlands*
[4]*Astrophysics Science Division, NASA Goddard Space Flight Center, Mail Code 661, Greenbelt, MD 20771, USA*
[5]*Joint Space-Science Institute, University of Maryland, College Park, MD 20742, USA*
[6]*Department of Physics, The George Washington University, 725 21st Street NW, Washington, DC 20052, USA*
[7]*Astronomy, Physics, and Statistics Institute of Sciences (APSIS), The George Washington University, Washington, DC 20052, USA*
[8]*Max-Planck Institut für extraterrestrische Physik, Giessenbachstr. 1, D-85740 Garching, Germany*
[9]*MIT Kavli Institute for Astrophysics and Space Research, Cambridge, MA 02139, USA*

Accepted 2019 October 25. Received 2019 October 25; in original form 2019 March 26

ABSTRACT

A small fraction of candidate tidal disruption events (TDEs) show evidence of powerful relativistic jets, which are particularly pronounced at radio wavelengths, and likely contribute non-thermal emission at a wide range of wavelengths. A non-thermal emission component can be diagnosed using linear polarimetry, even when the total received light is dominated by emission from an accretion disc or disc outflow. In this paper, we present Very Large Telescope (VLT) measurements of the linear polarization of the optical light of jetted TDE Swift J2058+0516. This is the second jetted TDE studied in this manner, after Swift J1644+57. We find evidence of non-zero optical linear polarization, $P_V \sim 8$ per cent, a level very similar to the near-infrared polarimetry of Swift J1644+57. These detections provide an independent test of the emission mechanisms of the multiwavelength emission of jetted TDEs.

Key words: techniques: polarimetric – galaxies: jets.

1 INTRODUCTION

In recent years, a multitude of tidal disruption event (TDE) candidates have been found in ultraviolet (UV) and optical wide-field surveys, some of which also showing bright X-ray emission (e.g. Komossa 2015). Generally, the optical and UV emission seems to follow a thermal spectrum, with temperatures in the region of $T \sim 10^4$ K. A rare subset of TDEs has been shown to produce powerful relativistic jets. To date, there are three firmly established relativistic TDEs: Swift J1644+57 (e.g. Bloom et al. 2011; Burrows et al. 2011; Levan et al. 2011), Swift J2058+0516 (e.g. Cenko et al. 2012; Pasham et al. 2015), and Swift J1112.2–8238 (Brown et al. 2015, 2017). In all three cases, the sources showed bright, rapidly variable, and long-lasting X-ray emission (brighter than commonly seen in thermal spectrum TDEs), and a bright radio counterpart. All three sources were first identified in data from the Burst Alert Telescope (BAT), a γ-ray instrument on board the *Neil Gehrels Swift Observatory* (hereafter *Swift*). Two of these sources have particularly good observational coverage: Swift J1644+57 and Swift J2058+0516. In both these cases, broad-band spectral energy distributions (SEDs) were obtained, spanning from low-frequency radio wavelengths all the way to high-energy γ-rays. The two sources differ somewhat in their optical and infrared behaviour: Swift J1644+57 shows high levels of extinction (e.g. Bloom et al. 2011; Burrows et al. 2011; Levan et al. 2011, 2016), making its optical and UV emission difficult to detect (Levan et al. 2016). Swift J2058+0516 suffers much less from extinction, resides in a fainter host, and is at far higher redshift ($z = 1.18$ versus $z = 0.34$) enabling the optical and rest-frame UV emission from the transient to be studied in greater detail. Pasham et al. (2015) show that the optical and infrared SED of Swift J2058+0516 can be described by a cooling blackbody-like spectrum in the rest frame, with a relatively constant radius, qualitatively similar to a large number of TDEs that are not seen to have relativistic jets, although significantly more luminous. The X-ray light curves of Swift J2058+0516 and Swift J1644+57 both show rapid variability at early times (e.g. Krolik & Piran 2011; Saxton et al. 2012; Pasham et al. 2015), and a very steep and sudden brightness drop half a year after the TDE γ-ray trigger (Pasham et al. 2015; Levan et al. 2016). The fast

★ E-mail: k.wiersema@warwick.ac.uk

Table 1. Log of VLT polarimetry observations of Swift J2058+0516. Uncertainties are 1σ and upper limits are given at 2σ level (see Section 2.1). The data quality of the acquisition image of the third epoch was too poor to measure a reliable magnitude. The discovery of the source by the Burst Alert Telescope (BAT) on *Swift* was on or around 2011 May 17 (MJD 55698), see Cenko et al. (2012) for details.

MJD date	Sequences[a]	Exp. time[b] (s)	TDE magnitude[c] (AB)	Seeing (arcsec)	$q(\times 100\%)$	$u(\times 100\%)$	$P(\times 100\%)$	θ (°)
55779.14848	3	300	23.21 ± 0.05	0.8	$2.20(\pm 1.86)$	$-1.36(\pm 1.04)$	<5.25	–
55862.07378	4	335	23.93 ± 0.07	1.5	$7.26(\pm 2.16)$	$4.40(\pm 3.31)$	$8.12(\pm 2.52)$	$15.6(\pm 8.51)$
55865.07486	4	335		0.9	$1.26(\pm 1.59)$	$-5.68(\pm 3.29)$	<12.88	–

[a]A sequence is defined as a set of exposures at four wave plate angles (0°, 45°, 22.5, and 67.5). [b]Exposure time per wave plate angle per sequence. [c]From acquisition images, calibrated on to the Panoramic Survey Telescope and Rapid Response System (Pan-STARRS) g-band values of field stars (Flewelling et al. 2016).

variability may provide a way to measure black hole masses, if the steep drop-off is associated with a transition from super-Eddington to sub-Eddington accretion regimes.

The detection rate of relativistic TDEs is low compared to the number of TDEs whose emission is generally thermal in the optical part of the spectrum (e.g. Saxton et al. 2019), and for which there is no relativistic jet component readily visible in the SED (see e.g. Auchettl, Guillochon & Ramirez-Ruiz 2017). To date, searches for non-thermal emission in thermal TDEs have largely focused on deep radio and X-ray searches (e.g. van Velzen et al. 2013), with a detection of a radio jet in at least one thermal TDE (Alexander et al. 2016; van Velzen et al. 2016). Similar to black hole X-ray binaries, a weak jet component may also be found through linear polarimetry at optical and near-infrared wavelengths (see Russell 2018 and references therein), which makes polarimetry an important additional diagnostic tool, independent of SED and light-curve models. Linear polarimetry has so far been limited to one jetted TDE (Swift J1644+57; Wiersema et al. 2012a) and one TDE without jet detection (OGLE 16aaa; Higgins et al. 2018). The infrared (K_s band) imaging polarimetry of Swift J1644+57 showed a sizeable degree of linear polarization ($P \sim 7.5 \pm 3.5$ per cent, measured after the initial steep decay phase and just prior a shallow decay phase, ∼18 d after trigger; see light curve in fig. 3 of Wiersema et al. 2012a), which motivated the polarimetric observations of Swift J2058+0516 presented in this paper.

In Section 2, we discuss the data reduction and calibration of our optical imaging polarimetry of Swift J2058+0516, and in Section 3, we compare our findings with those for Swift J1644+57 and recent numerical models.

2 OBSERVATIONS AND DATA ANALYSIS

2.1 VLT polarimetry

We observed Swift J2058+0516 using the FOcal Reducer/low dispersion Spectrograph 2 (FORS2) on the Very Large Telescope (VLT) of the European Southern Observatory (ESO), using its imaging polarimetry observing mode. Observations were obtained in Service mode. We acquired data at three epochs (Table 1), with each epoch consisting of a series of three or four individual wave plate angle sequences. Each sequence consisted of four exposures that were taken with a Wollaston element and a half-wave plate in the beam. The half-wave plate was rotated at angles of 0°, 45°, 22.5, and 67.5 within one sequence. The Wollaston element splits the incoming light into two, the ordinary and extraordinary beams, which are orthogonally polarized. A strip mask is used to prevent overlap of the ordinary and extraordinary beam images. All polarimetric observations used the ESO v_HIGH filter, and a 2 × 2 binning of the detector. We calculated the weighted average of all sequences per epoch to optimize our measurement signal-to-noise (S/N) ratio. The mid-times of the three epochs, the number of sequences, exposure times, and seeing conditions are listed in Table 1. The data quality of the second and third epoch is not optimal: there was poor seeing in epoch 2, and a high sky background (because of proximity to the Moon) in epoch 3.

Acquisition images were obtained as part of the target acquisition procedure for the polarimetry observations, used to place the target into the strip mask. All acquisition images used the filter v_HIGH. After data reduction, the acquisition images belonging to a single polarimetry epoch were combined, the source was well detected in epoch 1 and epoch 2 acquisition data, but only marginally in epoch 3 (due to the poor observing conditions). We used aperture photometry to extract fluxes, and calibrated these directly on to the Panoramic Survey Telescope and Rapid Response System (Pan-STARRS)[1] g-band values for field stars (ignoring colour terms). The light curve, including the acquisition image photometry and the photometry from Cenko et al. (2012) and Pasham et al. (2015), is shown in Fig. 1, with vertical dashed lines indicating the epochs of polarimetry. The light curve appears to show some degree of variability on top of a steady decline, with a steep drop at late times (Pasham et al. 2015). Note that a wide range of instruments (and calibrations) were used, and one should be cautious in interpretation of apparent features in this light curve.

The polarimetric data were reduced using routines in IRAF,[2] following the procedures outlined in Wiersema et al. (2014), using imaging flat-fields and bias frames taken as close in time to the science data as possible. Fluxes for the TDE and field stars were extracted using aperture photometry in the same manner as in Wiersema et al. (2014). We calculated the normalized Stokes parameters $q = Q/I$ and $u = U/I$ using a PYTHON 3[3] script following the method described in Patat & Romaniello (2006). These were then converted into the degree of linear polarization and the polarization angle, P and θ respectively, using the following relations:

$$P = \sqrt{q^2 + u^2}, \tag{1}$$

$$\theta = \frac{1}{2}\arctan\left(\frac{q}{u}\right) + \phi, \tag{2}$$

[1]https://panstarrs.stsci.edu
[2]Image Reduction and Analysis Facility (IRAF) is distributed by the National Optical Astronomy Observatories, which are operated by the Association of Universities for Research in Astronomy, Inc., under cooperative agreement with the National Science Foundation.
[3]www.python.org

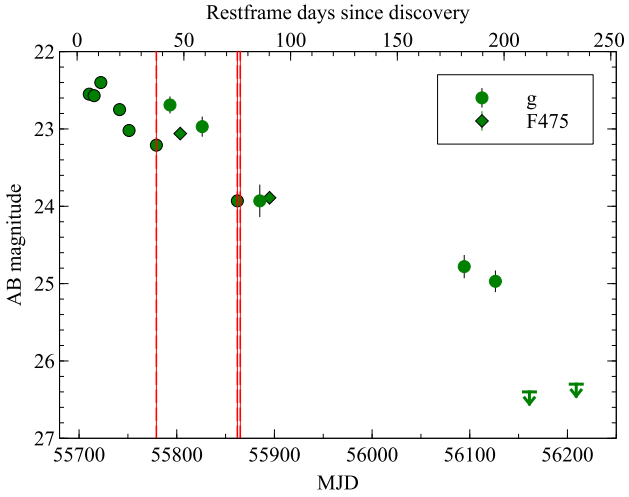

Figure 1. The optical light curve in g band, from Cenko et al. (2012) and Pasham et al. (2015), including data from Keck, the Gamma-Ray Burst Optical/Near-Infrared Detector (GROND), the William Herschel Telescope (WHT), Gemini-South, the Very Large Telescope (VLT), and the *Hubble Space Telescope* (*HST*). The vertical lines indicate the epochs of polarimetry, magnitudes from the acquisition images of the polarimetry sequences are added to the plot; magnitudes are not corrected for Galactic extinction. A steady decay with some variability is seen, with a steep drop at late times (Pasham et al. 2015).

$$\phi = \begin{cases} 0^\circ, & \text{if } q > 0 \text{ and } u \geq 0, \\ 180^\circ, & \text{if } q > 0 \text{ and } u < 0, \\ 90^\circ, & \text{if } q < 0, \end{cases} \quad (3)$$

where ϕ is an offset angle determined by the measured values of q and u (see Wiersema et al. 2012b). Note that we assume there is no polarimetric evolution within one epoch (i.e. we combine the sequences for each epoch together).

The measured linear polarization has to be corrected for polarization bias. The bias arises as linear polarization is derived from the addition of q and u in quadrature (see equation 1 or Serkowski 1958). There are a number of estimators that can correct for this bias, dependent on the S/N ratio (in flux and polarization) of the source (e.g. Simmons & Stewart 1985). We use the modified asymptotic (MAS) estimator described in Plaszczynski et al. (2014) to correct for the polarization bias. The generalized estimator is defined as follows:

$$P_{\rm MAS} = P - \sigma^2 \left[\frac{1 - {\rm e}^{\frac{-P^2}{\sigma^2}}}{2P} \right], \quad (4)$$

where $P_{\rm MAS}$ is the estimation of the true polarization P_0 and σ is the standard error on P. The variance on P can be found using the following relation:

$$\sigma^2 = \frac{u^2\sigma_u^2 + q^2\sigma_q^2}{q^2 + u^2}, \quad (5)$$

where σ_q and σ_u are the standard errors on q and u, respectively. Equation (5) assumes that q and u are independent.

For epochs where we have a positive detection of polarization (i.e. $P/\sigma \gtrsim 3$), the distribution of P is approximately Gaussian. Therefore, for our second epoch we can simply quote the 1σ errors. As the S/N ratio decreases, the distribution of P no longer follows a Gaussian distribution but instead follows a Rice distribution

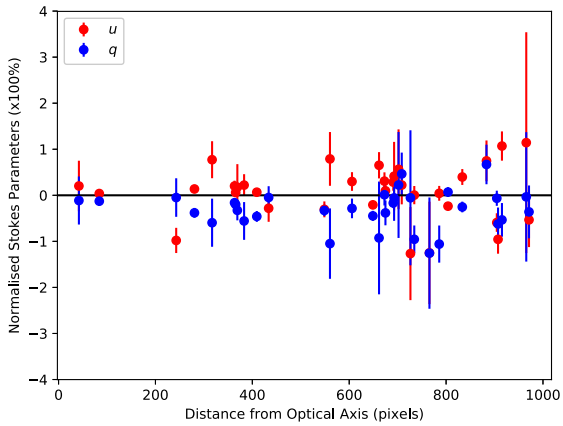

Figure 2. Plot representing the apparent normalized Stokes q and u polarizations of the unpolarized field stars away from the optical axis.

(Rice 1944; see also Patat & Romaniello 2006 for a numerical demonstration). This transition results in more complex confidence intervals for lower S/N ratios. We can calculate an upper limit on P using the following analytical relation from Plaszczynski et al. (2014):

$$P^{\alpha}_{\rm Upper} = P_{\rm MAS} + P_\alpha(1 - \beta\, {\rm e}^{-\gamma P_{\rm MAS}}), \quad (6)$$

where $\alpha = 0.95$, $P_\alpha = 1.95\sigma$, $\beta = 0.22$, and $\gamma = 2.54$ for a 2σ upper limit – which we quote for our first and third epochs. The measurements for all three epochs are shown in Table 1.

2.2 Off axis instrumental polarization/line-of-sight Galactic dust contribution

The intrinsic polarization of Swift J2058+0516 is not the only contributor to our measured polarization. Dust particles residing on our line-of-sight can induce a significant polarization signature through scattering. We attempted to quantify the Galactic dust contribution using field stars within the VLT field of view, assuming that the average intrinsic polarization of field stars is zero.

Our analysis included a total of 34 field stars at varying radial distances from the optical axis (where the TDE is placed). We calculated the q and u values utilizing the weighted average from all 11 observations over the three epochs to optimize our S/N ratio – as the stars are intrinsically unpolarized, the polarization signature in each epoch should be identical. The field stars are homogeneously distributed spatially around the optical axis and so we are confident that the summation of the contribution of instrumental polarization from all of these sources is negligible (the instrumental polarization likely has a weak radial pattern, increasing with radial distance from the optical axis; see e.g. Patat & Romaniello 2006; González et al., in preparation). The field stars chosen covered a range of magnitudes from ∼18 to 22.5 mag in the AB system. We opted for brighter sources to reduce the uncertainties on individual source measurements. Any measured offset in the centre of the Stokes q and u distribution should therefore come from the Galactic dust contribution. We calculated the polarization signature using the same method described in Section 2.1. Figs 2 and 3 show the field star q, u distribution. The resulting estimate for the Galactic line of sight contribution of the polarization is displayed in Table 2: we find a low value of $P < 0.48$ per cent, in line with expectations from the low line-of-sight Galactic dust extinction, $E(B-V) \approx 0.095$ mag (Schlafly & Finkbeiner 2011).

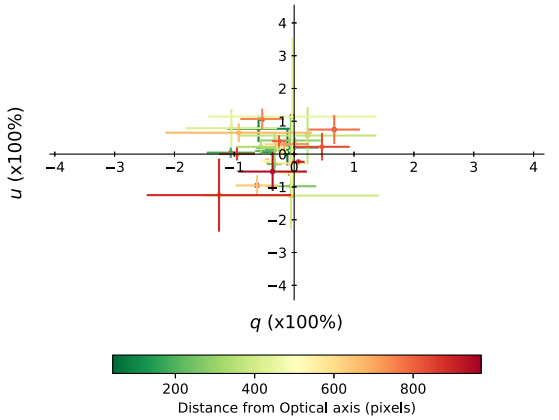

Figure 3. Plot representing the apparent polarization of unpolarized field stars in normalized Stokes q and u parameter space. This is caused due to the presence of instrumental polarization away from the optical axis. The colours represent the distance away from the optical axis.

Table 2. Estimation of the q, u, and P Stokes parameters induced by scattering by Galactic dust in the line of sight.

q (×100%)	u (×100%)	P (×100%)
−0.29(±0.10)	0.11(±0.15)	<0.48

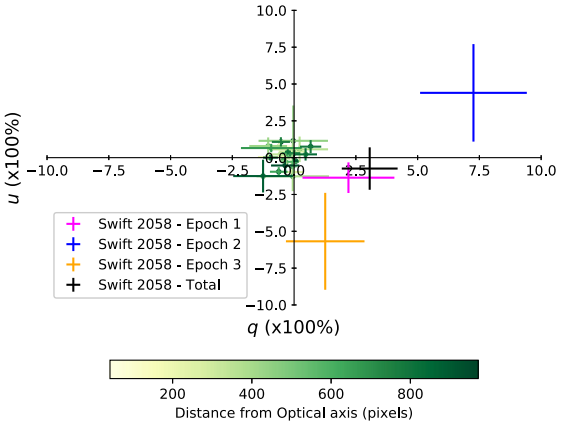

Figure 4. Plot showing the normalized Stokes q and u measurements for the three observational epochs of Swift J2058+0516 and the combined q and u measurements. The q and u values of the field stars are over plotted for comparison.

3 DISCUSSION

The measurements shown in Table 1 show a non-detection at epoch 1, a detection at epoch 2 ($P = 8.1 \pm 2.5$ per cent), and a non-detection at epoch 3. Epochs 2 and 3 are taken very close to each other, but conditions at epoch 3 were considerably poorer, and the 2σ limit for epoch 3 is consistent with the detected level in epoch 2. At epoch 1 we see a non-detection, with a 2σ limit of 5.3 per cent. This may imply some variation in P between epochs 1 and 2, which is more clearly seen in the q–u plane (Fig. 4), where epochs 2 and 3 appear more distinct. However, given the relatively large uncertainties, a constant level of P of ∼8 per cent (the level detected in epoch 2) cannot be confidently ruled out. We further note that we assumed there are no polarization variations at time-scales of a single observation epoch. If the polarization angle changes rotates fast compared to the duration of an observing epoch, the polarization would be smeared out and variation difficult to measure.

3.1 Comparison with Swift J1644+57

The only other jetted TDE with linear polarimetry measurements is Swift J1644+57. This source showed a non-zero linear polarization in the K_s band, of $P_{K_s} \sim 7.4 \pm 3.5$ per cent, measured using the William Herschel Telescope (WHT; Wiersema et al. 2012a). At first glance, the measured linear polarization of Swift J1644+57 and Swift J2058+0516 is remarkably similar, however there are some caveats to this comparison. First of all, the very high levels of dust extinction in the case of Swift J1644+57 likely imply a non-negligible contribution by dust scattering to the observed linear polarization, though it is very unlikely that all the polarization is caused by dust scattering in the host (Wiersema et al. 2012a). Secondly, the observations of Swift J1644+57 were done in the near-infrared K_s band and the source redshift is $z = 0.3543$ (Levan et al. 2011), the observations of Swift J2058+0516 were done in the v_HIGH filter and the source redshift is $z = 1.1853$ (Cenko et al. 2012). This means that for Swift J1644+57 the polarimetry was done in the rest-frame near-infrared, whereas for Swift J2058+0516 these were done in the rest-frame near-UV. These wavelength regimes may have somewhat different origins (Curd & Narayan 2019; see Section 3.3). Thirdly, the observations of Swift J1644+57 are obtained when the source showed a plateau-like light-curve evolution (fig. 3 in Wiersema et al. 2012a), whereas Swift J2058+0516 showed a somewhat more steady decline (Pasham et al. 2015).

3.2 Radio polarimetry

The relativistic jet physics of TDEs is arguably easiest to study at radio wavelengths, where the forward shock from the jet is bright. Indeed a rich phenomenology is seen that can be followed from just hours after the jet launch to years after. Abundant radio observations over a wide radio spectrum were obtained for Swift J1644+57 (Zauderer et al. 2011, 2013; Berger et al. 2012; Wiersema et al. 2012a; Cendes et al. 2014; Yang et al. 2016; Eftekhari et al. 2018). For Swift J2058+0516, the data set at radio wavelengths is considerably smaller (Cenko et al. 2012; Pasham et al. 2015) in terms of light curve and spectral coverage. In Wiersema et al. (2012a) we derived deep limits on the polarization of the radio emission of Swift J1644+57 (most sensitive 3σ limits as deep as 2.1 per cent), using deep observations with the Westerbork Synthesis Radio Telescope (WSRT), at a range of wavelengths and time-scales. To date, this remains the only published radio polarimetry data of a TDE. A small number of flux values at radio wavelengths for Swift J2058+0516 have been reported in the literature (Cenko et al. 2012; Pasham et al. 2015), using the Very Large Array (VLA) and the Very Long Baseline Array (VLBA), but we are unable to derive sensitive polarization measurements or limits for these observations, as insufficient polarization calibrator observations were obtained.

3.3 Comparison with models

It appears likely that the diversity in TDE emission is related to the dynamics and geometry of the accretion flow (with as key parameters the strength of the magnetic field around the black hole, the black hole mass, and the black hole spin parameter), the accretion rate, and the viewing angle. Optical emission may originate from a variety of mechanisms, e.g. from the accretion

disc, the jet, reprocessed X-ray emission, or from shocks generated by stellar debris self-crossing (Piran et al. 2015).

Dai et al. (2018) and Curd & Narayan (2019) present a set of three-dimensional general relativistic magnetohydrodynamic simulations to explore the impact of the various parameters on the resulting TDE spectra and light curves. Both groups find a relativistic jet is generated in some of their models. In particular, Curd & Narayan (2019) find that one of their models has a clear collimated relativistic outflow, with properties broadly consistent with those seen in jetted TDEs. The spectra computed by Curd & Narayan (2019) for the cases that do not produce a jet, match fairly well with observations of non-jetted TDEs, in particular reproducing the thermal components and properties of the X-ray emission. There are some discrepancies with observations and with the work from Dai et al. (2018) regarding the X-ray and optical emission for sources at different inclination angles. Curd & Narayan (2019) compare their simulation with data of Swift J1644+57, finding reasonable agreement with X-ray observations and jet structure, but the large, and uncertain, extinction in the line of sight of Swift J1644+57 precludes a comparison in the UV and optical range. Their model predictions indicate the presence of strong, beamed, X-ray and γ-ray emission from the jet. In the UV a thermal peak is predicted arising from the torus, with in the far-infrared a thermal synchrotron peak. In the optical domain the received light comes in part from the torus and in part from the outflow in the models of Curd & Narayan (2019), in proportions depending on the viewing angle.

An alternative model of TDE accretion and emission is presented by Coughlin & Begelman (2014). They argue that angular momentum of the infalling matter is too small to produce an accretion disc. Instead, the accretion energy is trapped and inflates the infalling gas to form a quasi-spherical 'Zero-Bernoulli Accretion' flow, or ZEBRA. ZEBRAs radiate as blackbodies, but can only do so up to the Eddington limit. Any additional accretion energy, injected into the inner regions of the ZEBRA by the black hole, is also unable to be efficiently advected to the surface inhibiting wind formation. Instead, this excess energy must escape as polar jets where the surface of the ZEBRA envelope can be exited. This model therefore accounts for both jetted and non-jetted TDEs as dependent on the observation angle, similarly to the unified model proposed by Dai et al. (2018). Swift J1644+57, Swift J1112.2–8238, and Swift J2058+0516 have all previously been examined in relation to the ZEBRA model (Coughlin & Begelman 2014; Wu, Coughlin & Nixon 2018). In particular, the ZEBRA model demonstrates a good agreement with the X-ray data for all three events, specifically the time-scale at which the X-ray flux drops as the accretion rate falls to sub-Eddington levels and the jet turns off, while the power-law spectrum and luminosity of Swift J1644+57's jet are consistent with the predictions from the ZEBRA model. During the jetted phase of Swift J2058+0516, the temperature of the thermal-like spectrum observed in the optical and UV is also consistent with the ZEBRA model, particularly with a black hole mass of $\sim 5 \times 10^6$ $M_\odot$, within the constraints found by Cenko et al. (2012). Comparing the ZEBRA model to non-jetted TDEs, Wu et al. (2018) find that the temperatures of $\sim$a few $\times 10^4$ K generally predicted are also more consistent with observations. In particular, there is a strong agreement with the SEDs of iPTF 16axa (Hung et al. 2017) and PS1 10jh (Gezari et al. 2012).

We may expect significant linear polarization for (optical) emission from the jet and for (inverse) Compton scattered emission, but much less so for the thermal torus emission. The forward shock emission (the interaction of the jet with external medium, not analysed in e.g. Curd & Narayan 2019) will be linearly polarized as well, with the amount depending on the jet structure (which is likely not homogeneous for at least Swift J1644+57; see e.g. Mimica et al. 2015), the viewing angle and the jet opening angle, and the detailed properties of the magnetic field in the shock, i.e. all the field random and confined to the shock, or is there an ordered component perpendicular to the shock – this is a well-studied problem in γ-ray burst afterglows (e.g. Gill & Granot 2018). At longer wavelengths, plasma propagation effects can give rise to significant depolarization of the forward shock radio emission (e.g. Toma et al. 2008). In addition to these internal effects, we are also likely to see the effect of dust scattering on the received polarization (see discussion in Wiersema et al. 2012a), which can polarize intrinsically unpolarized emission, convert linear to circular polarization (see discussion in Wiersema et al. 2014), and alter the linear polarization properties of intrinsically polarized light. In the case of Swift J1644+57 there is clear evidence of a large dust column, based on the very red colours of the transient light, whereas for Swift J2058+0516 the inferred amount of dust in the line of sight is far lower: Pasham et al. (2015) place a limit of $A_V \lesssim 0.2$ mag (assuming a Milky Way-like extinction law). This limit indicates that dust scattering along the line of sight is unlikely to contribute more than $\sim$1 per cent polarization at the observed wavelength (a more exact limit requires a better understanding of the dust grain size distribution). Our detection of linear polarization in Swift J2058+0516 at rest-frame blue optical/near-UV range indicates that some non-thermal emission is present in the received flux. The polarization P is moderate, and may be in agreement with the predicted flux origins by Curd & Narayan (2019), though a more quantitative comparison would require polarization measurements of a larger number of sources, at a larger number of wavelengths, and with smaller uncertainties.

3.4 Future TDE polarimetric follow-up

The sample of polarimetrically studied TDEs is very small. The predicted future TDE yield of large (optical) surveys like the Zwicky Transient Facility (ZTF) and Large Synoptic Survey Telescope (LSST) is large (LSST Science Collaboration 2009; Hung et al. 2018), and will allow a more systematic approach to TDE polarimetry in both optical and longer wavelengths. In Higgins et al. (2018) we trialled a linear polarimetry programme (the Snapshot survey for Polarised Light in Optical Transients, SPLOT) that obtained snapshot optical linear polarimetry of a large sample of randomly selected optical transients, which included a thermal TDE. A similar approach, using high-volume optical transient streams like the ZTF transient stream, and pre-selecting on nuclear transients, may greatly increase the yield of TDE polarimetry. It would simultaneously probe the effect of dust scattering in a statistical manner. A targeted optical polarimetric survey of TDE candidates with a high likelihood of having a relativistic jet, i.e. ones triggered by space-based X-ray or γ-ray detectors, or found in wide-field radio surveys (e.g. by MeerKAT; Booth et al. 2009), can further elucidate the origin of the different spectral components of TDEs. Optical and near-infrared spectropolarimetry would be a key extension to the imaging polarimetry presented in this paper and in Wiersema et al. (2012a). At the same time, a sample of thermal TDEs could remain valuable as a comparison, and has yet to be obtained. Since thermal TDEs are more common, and hence often at lower redshift, such observations can be obtained more readily. While limited to the brightest subsample (Swift J2058+0516 was too faint for optical spectropolarimetry throughout its evolution), the effects of dust scattering and the origin of the non-thermal emission

have different wavelength dependency, so spectropolarimetry would easily allow breaking of degeneracies, in a manner similar to spectropolarimetric studies of (core-collapse) supernovae.

In the X-ray regime, TDEs are an important component of the science cases for future X-ray polarimetry-capable missions such as the *Imaging X-ray Polarimetry Explorer* (*IXPE*) and *enhanced X-Ray Timing and Polarimetry* (*eXTP*; e.g. in 't Zand et al. 2019). The jetted TDEs are very bright at X-ray wavelengths, giving X-ray polarimetry with small statistical errors even at relatively short exposure times (in 't Zand et al. 2019), allowing tests for jet precession, the formation of globally ordered fields, and variations of the magnetic field over short time-scales (in 't Zand et al. 2019). At radio wavelengths, the advent of large, wide-field surveys (e.g. with the WSRT-APERture Tile In Focus, APERTIF; Oosterloo, Verheijen & van Capellen 2010) will provide a way to select jetted TDEs via their non-thermal radio emission, and collect polarization information for a large sample (APERTIF will survey the northern sky in polarized continuum). Deep circular radio polarimetry will similarly help test models for Faraday conversion in the jet, or in the intervening medium. Ultimately, the success of polarimetry for jetted TDEs will depend both the availability of suitable resources, and on the detection of candidates, which to date, have been rare.

4 CONCLUSIONS

In this paper, we present optical (V band) imaging polarimetry of Swift J2058+0516 using the VLT. This is only the second jet-driving, relativistic TDE studied using polarimetry, after Swift J1644+57. We obtained three epochs of data in which we find evidence of linear polarization in the second epoch, at a level $P = 8.1 \pm 2.5$ per cent, the other two epochs provide upper limits. There is weak evidence for polarization variation between the epochs. We compare the polarization information to current basic models, and find that these can accommodate small levels of linear polarization as measured. Our measurements of two relativistic TDEs show the value of linear polarimetry as a tool to better understand the contributions of disc, jet, and winds to the received spectrum. Polarimetry over a wider wavelength range will help to break existing degeneracies in comparison of models with light curve and broad-band SEDs.

ACKNOWLEDGEMENTS

We thank the anonymous referee for their constructive comments that improved this paper. This paper is based on observations collected at the European Organisation for Astronomical Research in the Southern Hemisphere under ESO programme 288.B-5011(A), PI: A. Levan. KW, AJL, and NRT acknowledge that this project has received funding from the European Research Council (ERC) under the European Union's Horizon 2020 research and innovation programme (grant agreement no. 725246). NRT, RLCS, ABH, and RAJE thank the STFC for support. RLCS acknowledges support from Royal Society Research Grant RG170230. KW thanks S. Covino for insightful discussion.

REFERENCES

Alexander K. D., Berger E., Guillochon J., Zauderer B. A., Williams P. K. G., 2016, ApJ, 819, L25
Auchettl K., Guillochon J., Ramirez-Ruiz E., 2017, ApJ, 838, 149
Berger E., Zauderer A., Pooley G. G., Soderberg A. M., Sari R., Brunthaler A., Bietenholz M. F., 2012, ApJ, 748, 36
Bloom J. S. et al., 2011, Science, 333, 203
Booth R. S., de Blok W. J. G., Jonas J. L., Fanaroff B., 2009, preprint (arXiv:0910.2935)
Brown G. C. et al., 2015, MNRAS, 452, 4297
Brown G. C. et al., 2017, MNRAS, 472, 4469
Burrows D. N. et al., 2011, Nature, 476, 421
Cendes Y. et al., 2014, preprint (arXiv:1412.3986)
Cenko S. B. et al., 2012, ApJ, 753, 77
Coughlin E. R., Begelman M. C., 2014, ApJ, 781, 82
Curd B., Narayan R., 2019, MNRAS, 483, 565
Dai L., McKinney J. C., Roth N., Ramirez-Ruiz E., Miller M. C., 2018, ApJ, 859, 20
Eftekhari T., Berger E., Zauderer B. A., Margutti R., Alexander K. D., 2018, ApJ, 854, 86
Flewelling H. A. et al., 2016, preprint (arXiv:1612.05243)
Gezari S. et al., 2012, Nature, 485, 217
Gill R., Granot J., 2018, MNRAS, 478, 4128
Higgins A. B. et al., 2019, MNRAS, 482, 5023
Hung T. et al., 2017, ApJ, 842, 29
Hung T. et al., 2018, ApJS, 238, 15
in 't Zand J. J. M. et al., 2019, Sci. China Phys. Mech. Astron., 62, 029506
Komossa S., 2015, J. High Energy Astrophys., 7, 148
Krolik J. H., Piran T., 2011, ApJ, 743, 134
Levan A. J. et al., 2011, Science, 333, 199
Levan A. J. et al., 2016, ApJ, 819, L51
LSST Science Collaboration, 2009, preprint (arXiv:0912.0201)
Mimica P., Giannios D., Metzger B. D., Aloy M. A., 2015, MNRAS, 450, 2824
Oosterloo T., Verheijen M., van Cappellen W., 2010, in Proceedings of the ISKAF2010 Science Meeting. Published online at http://pos.sissa.it/cgi-bin/reader/conf.cgi?confid=112, id.43
Pasham D. R. et al., 2015, ApJ, 805, 68
Patat F., Romaniello M., 2006, PASP, 118, 839
Piran T., Svirski G., Krolik J., Cheng R. M., Shiokawa H., 2015, ApJ, 806, 164
Plaszczynski S., Montier L., Levrier F., Tristram M., 2014, MNRAS, 439, 4048
Rice S. O., 1944, Bell Syst. Tech. J., 23, 282
Russell D., 2018, Galaxies, 6, 3
Saxton C. J., Soria R., Wu K., Kuin N. P. M., 2012, MNRAS, 422, 1625
Saxton R. et al., 2019, Astron. Nachr., 340, 351
Schlafly E. F., Finkbeiner D. P., 2011, ApJ, 737, 103
Serkowski K., 1958, Acta Astron., 8, 135
Simmons J. F. L., Stewart B. G., 1985, A&A, 142, 100
Toma K., Ioka K., Nakamura T., 2008, ApJ, 673, L123
van Velzen S., Frail D. A., Körding E., Falcke H., 2013, A&A, 552, A5
van Velzen S. et al., 2016, Science, 351, 62
Wiersema K. et al., 2012a, MNRAS, 421, 1942
Wiersema K. et al., 2012b, MNRAS, 426, 2
Wiersema K. et al., 2014, Nature, 509, 201
Wu S., Coughlin E. R., Nixon C., 2018, MNRAS, 478, 3016
Yang J., Paragi Z., van der Horst A. J., Gurvits L. I., Campbell R. M., Giannios D., An T., Komossa S., 2016, MNRAS, 462, L66
Zauderer B. A. et al., 2011, Nature, 476, 425
Zauderer B. A., Berger E., Margutti R., Pooley G. G., Sari R., Soderberg A. M., Brunthaler A., Bietenholz M. F., 2013, ApJ, 767, 152

This paper has been typeset from a TEX/LATEX file prepared by the author.